Available online at www.sciencedirect.com

ScienceDirect

Procedia Engineering 114 (2015) 94 – 101

Procedia Engineering

www.elsevier.com/locate/procedia

1st International Conference on Structural Integrity

Numerical evaluation of the direct method for cohesive law extraction in shear by the End-Notched Flexure test

R.L. Fernandes[a], R.D.S.G. Campilho[a,]*, A.C.C. Leitão[a], J.C.S. Azevedo[a]

[a]*Departamento de Engenharia Mecânica, Instituto Superior de Engenharia do Porto, Instituto Politécnico do Porto, Rua Dr. António Bernardino de Almeida, 431, 4200-072 Porto, Portugal.*

Abstract

With adhesive bonding, design can be oriented towards lighter structures, not only regarding the direct weight saving advantages of the joint over fastened or welded joints, but also because of flexibility to joint different materials. Cohesive Zone Models (CZM) are a powerful design tool, although the CZM laws of the adhesive bond in tension and shear are required as input in the models. This work evaluated the shear fracture toughness and CZM laws of bonded joints. The End-Notched Flexure (ENF) test geometry was used with this purpose. The experimental work consisted on the shear fracture characterization of the bond by conventional and the *J*-integral techniques. Additionally, by the *J*-integral technique, the precise shape of the cohesive law was defined. Numerical Finite Element (FE) simulations were carried out in Abaqus® to assess the accuracy of the obtained CZM laws in predicting the experimental behaviour of the ENF tests, with positive results. As output of this work, fracture data is provided in shear for the selected adhesive, allowing the subsequent strength prediction of bonded joints.

Peer-review under responsibility of INEGI - Institute of Science and Innovation in Mechanical and Industrial Engineering

Keywords: Cohesive zone models; finite element analysis; fracture mechanics; structural adhesive.

1. Introduction

With adhesive bonding, design can be oriented towards lighter structures, not only regarding the direct weight savings advantage over fastened or welded joints, but also because of flexibility to join different materials [1]. In the automotive industry, this gives a design advantage and better possibilities for optimization, resulting in weight

* Corresponding author. Tel.: +351 939526892; fax: +351 228321159.
E-mail address: raulcampilho@gmail.com

Peer-review under responsibility of INEGI - Institute of Science and Innovation in Mechanical and Industrial Engineering
doi:10.1016/j.proeng.2015.08.046

reduction and more competitive vehicles. Klarbring [2] showed by an asymptotic analysis that the behaviour of thin adhesive layers between stiff adherends is ruled by two straining modes: elongation, w, and shear, v (whose derivative variables are the normal stress, σ, and shear stress, τ, respectively). Although this is a simplification of the rigorous stress state at the adhesive layer, it is accurate for reproducing the macro-behaviour of adhesive layers [3]. One justification for this is that the Fracture Process Zone (FPZ) develops by a significant length beyond the crack tip, which makes the fracture toughness not particularly dependent of the precise details of stresses at the crack tip [4].

In any field of industry, the large-scale application of a given joint technique is based on the supposition that reliable tools for design and failure prediction are available. CZM is a particularly attractive technique, which assumes that the FPZ can be described at a macro-scale by a law relating the tractions and the physical separations at the crack tip. The cohesive laws are independently characterized for each loading mode and each transition in the global (mixed-mode) law is assessed by different criteria. Mode-mixicity is highly relevant for bonded joint failure analysis since cracks in adhesive joints propagate predominantly under mixed-mode. The capabilities of CZM modelling have led to the application of this technique to adhesively-bonded structures [5], in conjunction with different cohesive law shapes and improved cohesive law estimation techniques [3], [6]. The most important step in applying this technique is the estimation of the CZM laws [7]. A few data reduction techniques are currently available (the property determination technique, the direct method and the inverse method). In all cases, pure fracture tests, such as the Double-Cantilever Beam (DCB) for mode I and the ENF for mode II are employed. Data reduction methods for the tensile fracture toughness (G_n^c) by the DCB test are abundant, either conventional or not requiring crack length measurements [8]. The ENF test geometry is less addressed, yet conventional and plasticity accounting methods are available [9].

The property identification method is based on building a parameterized CZM law by isolated materials properties [4]. The inverse method relies on a trial and error fitting analysis to experimental data, such as the load-displacement (P-δ) curve of fracture tests [10]. Direct methods output the cohesive law directly from experimental data by measuring the J-integral and crack tip normal (δ_n) or shear displacements (δ_s) [11] by differentiation of the tensile strain energy release rate (G_n)–δ_n or shear strain energy release rate (G_s)–δ_s curves. In the work of Leffler et al. [12], the value of G_s^c and shear CZM law of an epoxy adhesive (DOW Betamate XW1044-3) were assessed experimentally by a J-integral methodology applied to the ENF specimen. The experimental procedure consisted on measuring the shear displacement at the crack tip by a digital camera attached to a microscope while recording the P-δ data. Results showed relatively consistent results for different values of adherend thickness. By comparing the resulting cohesive laws, results showed virtually identical values of shear stress, although the values of G_s^c were slightly different, on account of the varying shear deformation rates. A slightly different approach, but yet within the framework of the J-integral, is postulated by Stigh et al. [13], in which the adherends can deform plastically. This enables the specimen size to be reduced, but it requires the additional measurement of rotations at three locations in the ENF specimens.

This work evaluated the value of G_s^c of bonded joints. The experimental work consisted on the shear fracture characterization of the bond by conventional and J-integral techniques. Additionally, by the J-integral technique, the precise shape of the cohesive law was defined. FE simulations were carried out in Abaqus® to assess the accuracy of the obtained CZM laws in predicting the experimental behaviour of the ENF tests.

2. Experiments

2.1. Materials

The aluminium alloy AA6082 T651 was selected. This is a highly ductile aluminium alloy, as shown by the mechanical properties obtained in the work of Campilho et al. [14]: Young's modulus (E) of 70.07±0.83GPa, tensile yield stress (σ_y) of 261.67±7.65MPa, tensile failure strength (σ_f) of 324±0.16MPa and tensile failure strain (ε_f) of 21.70±4.24%. The experimental stress-strain (σ-ε) curves and the numerical approximation, to be used further in

work, are presented in Fig. 1. The ductile epoxy adhesive Araldite® 2015 was selected. A comprehensive mechanical and fracture characterization was undertaken [3], [11], [14]. Bulk specimens in tension enabled obtaining E, σ_y, σ_f and ε_f. G_n^c and G_s^c were obtained by conventional data reduction schemes using the DCB and ENF tests, respectively.

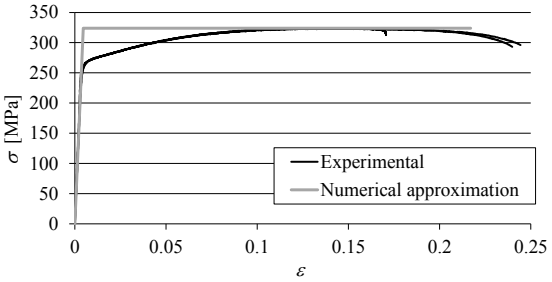

Fig. 1: σ-ε curves of the aluminium: experimental data and numerical approximation.

2.2. Joint geometry

Fig. 2 shows the characteristic geometry and dimensions of the ENF joints: mid-span L=100mm, initial crack length a_0≈60 mm, adherend thickness t_P=3mm, width b=25mm and adhesive thickness t_A=0.2mm.

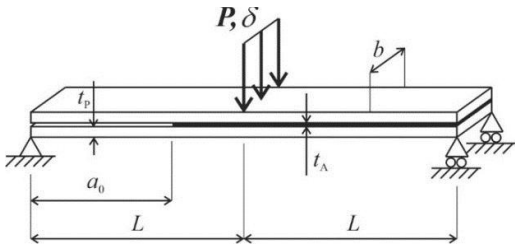

Fig. 2: ENF specimens' geometry and relevant dimensions.

Before bonding, the adherends faces to join were roughened by grit blasting followed by cleaning with acetone. Calibrated steel spacers were inserted between the adherends to obtain a constant value of t_A in the adhesive bond. Curing was performed at room temperature. Final set-up of the specimens was then undertaken with the removal of the steel spacers, painting the crack tip path with brittle white paint, and gluing a black numbered scale in both upper and lower adherends to aid the parameter extraction for the direct method. The tests were carried out at room temperature in a Shimadzu AG-X 100 testing machine equipped with a 100kN load cell. For the required test documentation, a 18MPixel digital camera was used.

2.3. Data reduction methods for G_s^c

In this work, apart from the J-integral, the following conventional techniques were tested: Compliance Calibration Method (CCM), Direct Beam Theory (DBT), Corrected Beam Theory (CBT) and Compliance-Based Beam Method (CBBM). For the formulae and detailed discussion of these conventional methods, the reader can refer to reference [9]. The direct method relies on the simultaneous measurement of the J-integral and δ_s [12]. The proposed G_s evaluation expression results from using alternate integration paths to extract the J-integral [15], resulting on the following closed-form expression for G_s [12]:

$$G_s = \frac{9}{16}\frac{\left(P_u a\right)^2}{E_a t_P^{\,3}} + \frac{3}{8}\frac{P_u \delta_s}{t_P}, \tag{1}$$

where P_u is the current load per unit width at the loading cylinder, a the crack length and E_a the Young's modulus of the adherends. The current shear traction (t_s)-δ_s plot or shear cohesive law of the adhesive layer is estimated by fitting of the resulting G_s-δ_s curve and differentiation with respect to δ_s [12]

$$t_s(\delta_s) = \frac{\partial G_s}{\partial \delta_s}. \quad (2)$$

2.4. Experimental results

2.4.1. Conventional methods

The G_s^c values were estimated by the data reduction methods mentioned in Section 2.3. The *R*-curves, which relate G_s vs. a, are shown in Fig. 3, considering a representative specimen. For all data reduction techniques the *R*-curve is consistent with the theoretically steady-state value of G_s that should be obtained throughout the crack growth phase. Another distinctive feature that is patent in Fig. 3 is the deviation to the right of the CBBM curve relatively to the techniques requiring a measurement, which is justified by the inclusion of the FPZ in the equivalent crack length (a_{eq}) used by this method, thus rendering the real crack longer than the measured one [9].

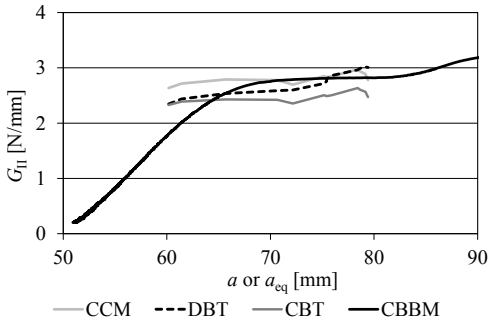

Fig. 3: *R*-curves for all conventional methods for a representative specimen.

By comparing the curves by the different methods, the CBT clearly under predicts the CCM, DBT and CBBM. Table 1 summarizes the values of G_s^c [N/mm] of all specimens, considering the average G_s value during the steady-state portion of the curve, and respective average values and deviation for each data reduction technique. For space saving purposes, the *J*-integral values, to be addressed further, are also presented. Between specimens of the same method, results agree quite well. Additionally, the results between data reduction methods were consistent except for the CBT. Considering the CBBM values as reference, the CBT under predicts these values by 17.0%.

Table 1: Values of G_s^c [N/mm] by all conventional methods and the *J*-integral

Adhesive	Araldite® 2015				
Specimen	CCM	DBT	CBT	CBBM	*J*-integral
1	3.029	3.083	2.644	3.420	3.444
2	-	-	-	-	3.585
3	3.675	2.401	2.177	2.545	2.873
4	3.214	2.916	2.544	2.943	3.298
5	2.812	2.741	2.476	2.801	3.123
6	3.357	3.088	2.644	3.136	3.140
7	2.696	2.831	2.624	2.901	3.080
8	3.008	2.952	2.512	3.025	2.901
Average	3.113	2.859	2.517	2.967	3.181
Deviation	0.334	0.238	0.164	0.273	0.249

[a] Polynomial fitting difficulties

2.4.2. J-integral

Initially, the value of δ_s was obtained with 5 s intervals for each test specimen, following an automatic data extraction procedure described in reference [11]. Fig. 4 gives a representative example of the variation of δ_s with the time elapsed since the beginning of the test.

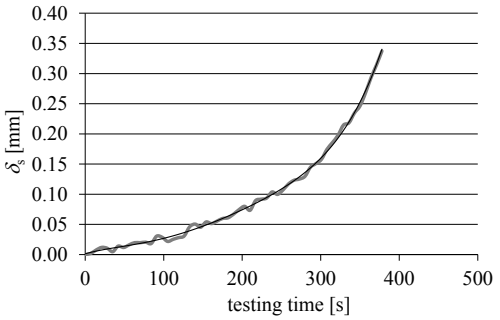

Fig. 4: δ_s – testing time curve for a specimen up to crack initiation with polynomial approximation.

The raw curve and the adjusted polynomial law are presented in Fig. 4. Depending of the specimen under analysis, different degree polynomials were selected in order to attain the best correlation factor, R (which is also valid for the polynomial to fit the G_s-δ_s law). The evolution of δ_s in Fig. 4 is exponential with the testing time. After having the δ_s-testing time plots, it was possible to estimate the G_s-δ_s relationship by direct application of equation (1) . The G_s^c estimate is given by the steady-state value of G_s in the G_s-δ_s curve, which corresponds to the onset of crack propagation.

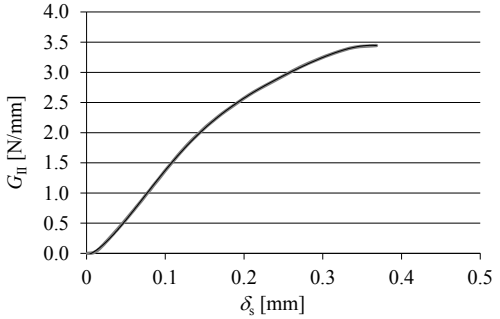

Fig. 5: G_s – δ_s curve for a specimen up to crack initiation with polynomial approximation.

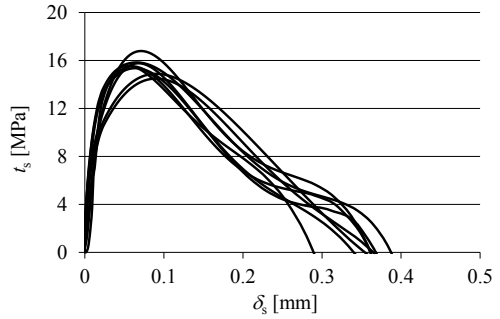

Fig. 6: t_s-δ_s curves obtained by the direct method.

Fig. 5 shows the G_s-δ_s curve for the same specimen of Fig. 4 and the selected polynomial approximation. For the specimen depicted in the figures, the measured value of G_s^c [N/mm] is 3.444. The overall results for all specimens are presented in Table 1. These reveal a good repeatability, with a percentile deviation of 7.83%. The results are consistent with the CBBM, with a deviation between average values of 7.21%. To apply the differentiation procedure represented by equation (2), polynomial functions were applied to the raw data of each specimen. Fig. 6 shows the full set of t_s-δ_s curves obtained by the direct method. The average and deviation of the cohesive parameters (with percentile deviation in parenthesis) were as follows: shear cohesive strength t_s^0=15.5±0.683MPa (4.4%), maximum strength displacement δ_s^0=0.0702±0.0122mm (17.4%) and failure displacement δ_{sc}=0.372±0.0246mm (6.6%). Fig. 7 compares a typical CZM law for the adhesive Araldite® 2015 and triangular and trapezoidal CZM approximations. This adhesive is best modelled by a trapezoidal CZM law, although it can also be modelled with a triangular CZM law as well.

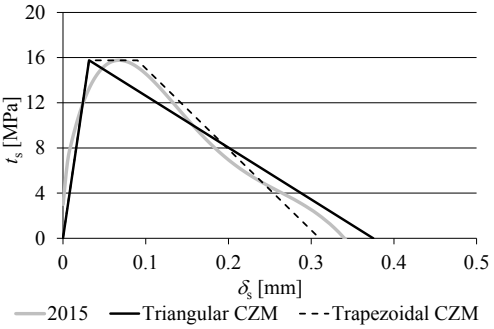

Fig. 7: Example of t_s-δ_s curve with triangular and trapezoidal approximations.

3. Numerical analysis

3.1. Analysis conditions

A numerical FE analysis of the ENF tests was carried out in Abaqus® aiming to reproduce the experimental results by using the obtained CZM laws. The analysis is geometrically non-linear. Fig. 8 shows the applied boundary and loading conditions. The FE mesh was built considering plane-strain four-node quadrilateral solid finite elements for the adherends, while the adhesive layer was modelled with four-node cohesive elements, including a bilinear (triangular) CZM since it is readily available in the software. Each adherend was modelled by six elements in the thickness direction, with a more refined mesh near the adhesive region [16], [17]. In the adhesive layer region and near the cylinders a more refined mesh was used, considering 0.20 mm and 0.05 length elements, respectively. The boundary conditions are also shown in Fig. 8 and they consisted in fixing the supporting cylinders and restraining the loading cylinder in the horizontal direction.

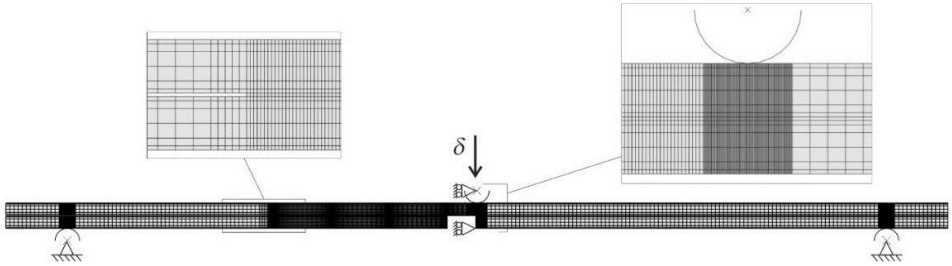

Fig. 8: Applied boundary and loading conditions on the meshed model of an ENF joint.

3.2. Triangular CZM formulation

CZM are based on a relationship between stresses and relative displacements connecting homologous nodes of the cohesive elements, to simulate the elastic behaviour up to a peak load and subsequent softening, to model the gradual degradation of material properties up to complete failure. The areas under the traction-separation laws in tension and shear are equalled to G_n^c and G_s^c, respectively. Under pure mode, damage propagation occurs at a specific integration point when the stresses are released in the respective traction-separation law. Under mixed mode, energetic criteria are often used to combine tension and shear [18]. In this work, the quadratic nominal stress criterion was considered for the initiation of damage. After the peak value is attained, the material stiffness is degraded. Complete separation is predicted by a linear power law form of the required energies for failure in the pure modes. For full details of the presented model, the reader can refer to reference [14].

3.3. Simulation results

The numerical models were built individually for each specimen considering their particular dimensions, namely a_0. The shear CZM law obtained by the direct method for each individual specimen was input in the models by performing a triangular approximation. The elastic stiffness was calculated by the E value defined for this adhesive and t_A=0.2mm. The value of t_s^0 was equaled to the maximum value of the t_s-δ_s curve and G_s^c was obtained by the J-integral measurement shown in Table 1. The value of δ_{sc} was computed internally, knowing that the area under the CZM law is given by G_s^c. Fig. 9 shows a curve fitting example between numerical and experimental P-δ curves of an ENF specimen, showing the overall agreement between the experimental P-δ curves and numerical approximations after applying the individually obtained CZM laws in shear by the direct method. For this specimen, the percentile difference between maximum P values is 0.26%, and 0.92% for the respective δ values. For the complete set of tested specimens, the average of the individual absolute differences of these two quantities is 0.42% and 0.96%, by the same order as depicted above.

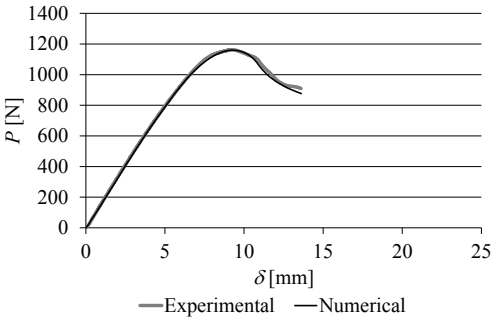

Fig. 9 – Curve fitting example between numerical and experimental P-δ curves of an ENF specimen.

Apart from this verification, the effect of each of the CZM parameters was assessed on the outcome of the predicted P-δ curves. The results were as follows: (1) the E value of the adherends influences the elastic slope of the curve, (2) G_s^c affects the peak value of P by translation of the descending part of the curve (without changing the elastic slope) and (3) t_s^0 slightly increases the peak load and highly affects the specimen stiffness up to the peak load, leading to a more abrupt post-peak load reduction with the increase of t_s^0 [9]. On account of this behaviour, it can be concluded that a unique CZM law exists for each specimen and, as it can be observed in Fig. 9, the triangular CZM managed to capture with accuracy the adhesive layer of Araldite® 2015. It could be argued that a different CZM shape is better suited to capture the ductility of the Araldite® 2015. However, since damage growth is ruled by the fracture energies instead of the stresses, the triangular CZM showed good results as well.

4. Conclusions

This work addressed the calculation of G_s^c and shear CZM law of an adhesive layer of Araldite® 2015, considering the ENF test. Validation of the individual CZM law for each specimen was undertaken numerically, aiming to the reproduce the experimental P-δ curves. The tested methods to estimate G_s^c were the CCM, DBT, CBT, CBBM and J-integral. All methods showed a good agreement between specimens. However, between methods the CBT showed smaller values of G_s^c. Application of the J-integral, although allowing the estimation of the CZM law by differentiation of the $G_s=f(\delta_s)$ curve, is based on the measurement of δ_s, which requires a high-precision technique on account of the very small values of this parameter up to crack initiation. However, it has the big advantage of providing complete data (in this case in shear) for strength prediction by CZM modelling. The CZM laws of the tested adhesive revealed a good agreement between specimens. The numerical reproduction of the ENF tests, namely the P-δ curves, showed that the obtained CZM laws are highly accurate in prediction the joints' behavior in shear. Together with tensile characterization data of this adhesive and mixed-mode damage initiation and propagation criteria, it is possible to predict the strength of bonded joints under generic loading conditions by CZM modelling.

References

[1] L.F.M. da Silva, A. Öchsner, R.D. Adams, (eds). Handbook of adhesion technology, Springer, Heidelberg, 2011.

[2] A. Klarbring, Derivation of a model of adhesively bonded joints by the asymptotic expansion method. Int. J. Eng. Sci. 29 (1991) 493-512.

[3] R.D.S.G. Campilho, M.D. Banea, J.A.B.P. Neto, L.F.M. da Silva, Modelling adhesive joints with cohesive zone models: effect of the cohesive law shape of the adhesive layer, Int. J. Adhes. Adhes. 44 (2013) 48-56.

[4] T. Andersson, U. Stigh, The stress–elongation relation for an adhesive layer loaded in peel using equilibrium of energetic forces, Int. J. Solids Struct. 41 (2004) 413-434.

[5] M.F.S.F. de Moura, J.P.M. Gonçalves, J.A.G. Chousal, R.D.S.G. Campilho, Cohesive and continuum mixed-mode damage models applied to the simulation of the mechanical behaviour of bonded joints, Int. J. Adhes. Adhes. 28 (2008) 419-426.

[6] R.D.S.G. Campilho, M.D. Banea, J.A.B.P. Neto, L.F.M. da Silva, Modelling of single-lap joints using cohesive zone models: effect of the cohesive parameters on the output of the simulations, J. Adhes. 88 (2012) 513-533.

[7] M.J. Lee, T.M. Cho, W.S. Kim, B.C. Lee, J.J. Lee, Determination of cohesive parameters for a mixed-mode cohesive zone model, Int. J. Adhes. Adhes. 30 (2010) 322-328.

[8] M.F.S.F. de Moura, R.D.S.G. Campilho, J.P.M. Gonçalves, Crack equivalent concept applied to the fracture characterization of bonded joints under pure mode I loading. Compos. Sci. Technol. 68 (2008) 2224-2230.

[9] M.F.S.F. de Moura, R.D.S.G. Campilho, J.P.M. Gonçalves, Pure mode II fracture characterization of composite bonded joints, Int. J. Solids Struct. 46 (2009) 1589-1595.

[10] R.D.S.G. Campilho, M.F.S.F. de Moura, A.M.G. Pinto, J.J.L. Morais, J.J.M.S. Domingues, Modelling the tensile fracture behaviour of CFRP scarf repairs, Compos. Part B 40 (2009) 149-157.

[11] R.D.S.G. Campilho, D.C. Moura, D.J.S. Gonçalves, J.F.M.G. da Silva, M.D. Banea, L.F.M. da Silva, Fracture toughness determination of adhesive and co-cured joints in natural fibre composites, Compos. Part B 50 (2013) 120-126.

[12] K. Leffler, K.S. Alfredsson, U. Stigh, Shear behaviour of adhesive layers, Int. J. Solids Struct. 44 (2007) 530-545.

[13] U. Stigh, K. Alfredsson, A. Biel, Measurement of cohesive laws and related problems. In: Proceedings of the ASME Int Mech Eng Congress and Exposition, 2009.

[14] R.D.S.G. Campilho, M.D. Banea, A.M.G. Pinto, L.F.M. da Silva, A.M.P. de Jesus, Strength prediction of single- and double-lap joints by standard and extended finite element modelling, Int. J. Adhes. Adhes. 31 (2011) 363-372.

[15] J.R. Rice, A path independent integral and the approximate analysis of strain concentration by notches and cracks, J. Appl. Mech. 35 (1968) 379-386.

[16] R.D.S.G. Campilho, M.F.S.F. de Moura, A.M.J.P. Barreto, J.J.L. Morais, J.J.M.S. Domingues, Fracture behaviour of damaged wood beams repaired with an adhesively-bonded composite patch, Compos.: Part A – Appl. Sci. 40 (2009) 852-859.

[17] H.R. Daghyani, L. Ye, Y.W. Mai, Mixed-mode fracture of adhesively bonded CF/Epoxy composite joints, J. Compos. Mater. 30 (1996) 1248-1265.

[18] M. Ridha, V.B.C. Tan, T.E. Tay, Traction-separation laws for progressive failure of a bonded scarf repair of composite panel, Compos. Struct. 93 (2010) 1239-1245.